THE ROYAL SOCIETY

J. R. Soc. Interface (2004) **1**, 17–22
DOI: 10.1098/rsif.2004.0003

The mechanism of biomineralization of bone-like apatite on synthetic hydroxyapatite: an *in vitro* assessment

Hyun-Min Kim[1,†], Teruyuki Himeno[2], Masakazu Kawashita[2], Tadashi Kokubo[3] and Takashi Nakamura[4]

[1]*Department of Ceramic Engineering, School of Advanced Materials Engineering, Yonsei University, 134 Shinchon-dong, Seodaemun-gu, Seoul 120-749, Korea*
[2]*Department of Material Chemistry, Graduate School of Engineering, Kyoto University, Katsura, Nishikyo-ku, Kyoto 615-8510, Japan*
[3]*Research Institute of Science and Technology, Chubu University, 1200 Matsumoto-cho, Kasugai-shi, Aichi 487-8501, Japan*
[4]*Department of Orthopaedic Surgery, Graduate School of Medicine, Kyoto University, Shogoin, Sakyo-ku, Kyoto 606-8507, Japan*

The mechanism of biomineralization of bone-like apatite on synthetic hydroxyapatite (HA) has been investigated *in vitro*, in which the HA surface was surveyed as a function of soaking time in simulated body fluid (SBF). In terms of surface structure by transmission electron microscopy with energy-dispersive X-ray spectrometry, the HA whose Ca/P atomic ratio was 1.67 revealed three different characteristic soaking periods in SBF, i.e. the first soaking period, in which the HA surface increased the Ca/P ratio up to 1.83 to form an amorphous phase of Ca-rich calcium phosphate; the second soaking period, in which the HA surface decreased the Ca/P ratio up to 1.47 to form an amorphous phase of Ca-poor calcium phosphate; and the third soaking period, in which the HA surface gradually increased the Ca/P ratio up to 1.65 to eventually produce the bone-like nano-cerystallites of apatite, which grew forming complex crystal assemblies with a further increase in immersion time. Analysis using electrophoresis spectroscopy indicated that, immediately after immersion in SBF, the HA revealed a highly negative surface potential, which increased to reach a maximum positive value in the first soaking period. The surface potential then decreased to again reach a negative value in the second soaking period and thereafter converge to a constant negative value in the third soaking period. This implies that the HA induces biomineralization of apatite by smartly varying its surface potential to trigger an electrostatic interaction, first with positive calcium ions and second with negative phosphate ions in the SBF.

Keywords: hydroxyapatite; biomineralization; calcium phosphate; bioactivity; simulated body fluid (SBF); surface potential

1. INTRODUCTION

Apatite is the major mineral phase of which the hard tissue such as bone and dentin in the human body is composed. The biomineralization of apatite, which in hard tissue is usually a self-remodelling process guided by bone cells and proteins, has also been documented to occur on surfaces of some synthetic ceramics of crystalline calcium phosphate and amorphous silicates and titanates (Kokubo 1991, 1992; Hench 1991; Kim 2001; Ohtsuki *et al.* 1991; Ohura *et al.* 1991; Neo *et al.* 1992, 1993). These ceramics are so-called bioactive ceramics and, in fact, they smartly utilize the apatite that is mineralized on their surfaces as an interface to integrate spontaneously with living tissue (Ohtsuki *et al.* 1991; Ohura *et al.* 1991; Kokubo 1992; Neo *et al.* 1992, 1993).

†Author for correspondence (hmkim@yonsei.ac.kr).

The bioactive ceramics have not only granted us distinguished bone-repairing biomaterials, such as Bioglass®, sintered hydroxyapatite (HA) and glass–ceramic A–W (Hench *et al.* 1971; Jarcho *et al.* 1977; Kokubo *et al.* 1982), but also are inspiring bio-interactive materials with enhanced or novel physical, chemical and biological functions (Hench 1998; Kokubo *et al.* 2003), for which a key requirement is the mechanism of biomineralization of apatite on the known bioactive ceramics.

The biomineralization of apatite on a bioactive ceramic is considered to be a consequence of a ceramic surface reaction with interstitial blood plasma, of which the core cascade appears inorganic. Specifically *in vitro*, an acellular simulated body fluid (SBF) with ion concentrations nearly equal to those in blood plasma could reproduce the formation of apatite on bioactive ceramics *in vivo* (Kokubo *et al.* 1989, 1990;

Received 15 April 2004
Accepted 7 May 2004
Published online 24 May 2004

Kim *et al.* 1996; Ebisawa *et al.* 1993; Filguerias *et al.* 1993). Biomimetic assessments using SBF have shown that bioactive silicates or titanates use surface functional groups composed of Si-OH or Ti-OH to induce the formation of apatite on their surfaces (Ohtsuki *et al.* 1992, 1995; Kim *et al.* 1995, 1996b; Li *et al.* 1992, 1994). More recently, these functional groups have been shown to induce the formation of apatite indirectly, through formations of early precursors of amorphous calcium silicate or calcium titanate and late precursors of amorphous calcium phosphate, which eventually crystallize into apatite with bone mineral-like compositions and structures (Takadama *et al.* 2001a, 2001b, 2002; Coreño *et al.* 2001). This cascade was speculated as being involved with the electrostatic interaction of the surface functional groups with the calcium and phosphate ions in the fluid. The mechanism of the biomineralization of apatite in this context is particularly interesting in relation to the sintered HA in view of its compositional similarity to bone mineral and biomedical popularity, but such scientific information is rare.

This study investigates the variations in surface composition, structure and potential of HA in the process of biomineralization of apatite on its surface in an *in vitro* model using SBF. The HA surface was surveyed using transmission electron microscopy (TEM), along with energy-dispersive X-ray spectrometry (EDX) as well as laser electrophoresis spectroscopy as a function of immersion time in SBF. The pathway of biomineralization of apatite on HA is discussed in terms of changes in surface composition and structure, where the mechanism is rationalized in terms of changes in surface potential.

2. MATERIALS AND METHODS

2.1. Materials and in vitro model

The starting material was typical dense HA polycrystals (Mitsubishi Materials Co., Tokyo, Japan), which was prepared by conventional sintering of powder compaction at 1200 °C. The bulk HA was pulverized by dry ball milling in a high-purity zirconia pot, and sieve-screened into particles less than 5 μm in size. The solution for *in vitro* modelling was SBF (Kokubo *et al.* 1990) with a pH of 7.40 and ion concentrations nearly equal to those of human blood plasma (Na^+ 142.0, K^+ 5.0, Mg^{2+} 1.5, Ca^{2+} 2.5, Cl^- 147.8, HCO_3^- 4.2, HPO_4^{2-} 1.0, SO_4^{2-} 0.5 mM). The SBF was prepared by dissolving reagent-grade chemicals of NaCl, $NaHCO_3$, KCl, $K_2HPO_4{\cdot}3H_2O$, $MgCl_2{\cdot}6H_2O$, $CaCl_2$ and Na_2SO_4 (Nacalai Tesque Inc., Kyoto, Japan) in distilled water and buffering at a pH of 7.40 with tris(hydroxymethyl)aminomethane ($(CH_2OH)_3CNH_3$) and 1.0 M hydrochloric acid (Nacalai Tesque Inc., Kyoto, Japan) at 36.5 °C. The HA particles of 50 mg in mass were immersed and soaked in 120 ml of SBF at 36.5 °C.

2.2. Methods of surface characterizations

The surface composition and structure of the HA before and after soaking in SBF were analysed using TEM (JEM-2000FXIII, JEOL,Co., Tokyo, Japan) along with EDX (VOYAGER III, NORAN Instruments, Inc., Middletown, WI). After soaking for various periods, the HA particles removed from the SBF were dispersed in ethanol and deposited onto poly(vinylformal) film supported by a 200 mesh, 3 mm diameter nylon grid. TEM observations were performed, finding sharp edge spots of the HA particles to present two-dimensional images. In particular in EDX analysis, the as-measured results were calibrated using extra pure reagent references of tricalcium phosphate ($Ca_3(PO_4)_2$; Nacalai Tesque Inc., Kyoto, Japan) and HA ($Ca_{10}(PO_4)_6(OH)_2$; Sigma Chemical Co., Ltd., St. Louis, MO).

The surface potential of the HA after immersion in SBF was analysed in terms of its zeta potential, which was measured using laser electrophoresis spectroscopy (Model ELS9000K, Otsuka Electronics Co., Osaka, Japan). After they were removed from the SBF, the HA particles were dispersed into fresh SBF in a high-purity silica glass cell, which was immediately equipped into the electrophoresis system to measure the zeta potential of the HA surface. This system adopts laser Doppler electrophoresis to measure the electrophoretic mobility of HA particles. The zeta potential (ζ) is given by the Smoluchowski equation,

$$\zeta = 4\pi\eta U/\varepsilon, \tag{2.1}$$

where U is the electrophoretic mobility of HA, η is the viscosity of the solution and ε is the dielectric constant of the solution. As long as the HA particles are floating in the solution, the electrophoretic mobility (U) depends neither on the size nor the shape of the particles, but solely on the current of electro-osmosis by the zeta potential of the HA (van de Ven 1989). At each condition of immersion time, the zeta potential was measured at least five times to present an average value with standard deviation.

3. RESULTS

Figures 1–6 show the TEM–EDX profiles of the surfaces of the HA before and after soaking in SBF for various periods. The TEM image for each soaking time is representative of those observations on several sites of the HA surface. The asterisks indicate the centres of the electron diffraction and EDX analysis areas, which are around 100 nm in diameter. The TEM image of HA before soaking in SBF (0 h, see figure 1) showed the mill-fractured surface of a HA particle, where the EDX detected Ca, P, O and C, among which the C is revealed by the polymer film and grid supporting the HA particles. The Ca/P atomic ratio of the specimen HA was exactly 1.67, as was expected by the stoichiometric composition of HA ($Ca_{10}(PO_4)_6(OH)_2$). The electron diffraction revealed typical dot patterns of polycrystalline ceramics, which are arranged on ring indexes indicating the (002), (211) and (213) planes of the HA crystal (see the inset in figure 1).

After soaking in SBF for 3 h (see figure 2), an electron-lucent product was observed on the HA in the TEM image. The EDX elements of this product were the same as those before soaking, but the Ca/P ratio drastically increased to 1.74. In the electron diffraction,

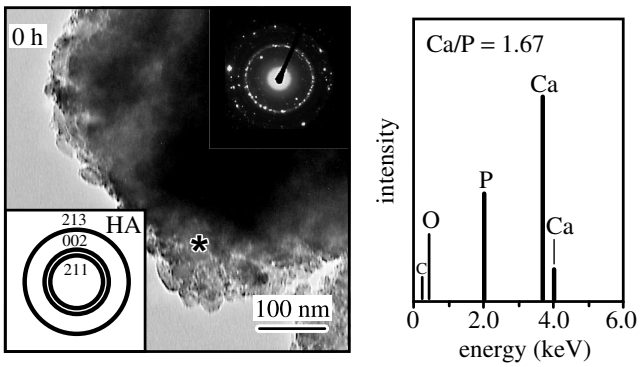

Figure 1. TEM–EDX profile of the surface of HA before soaking in SBF (∗: centre of electron diffraction and EDX; inset: index of electron diffraction pattern of HA).

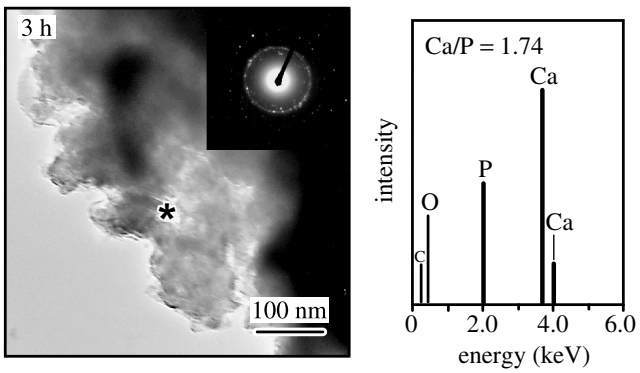

Figure 2. TEM–EDX profile of the surface of HA after soaking in SBF for 3 h (∗: centre of electron diffraction and EDX).

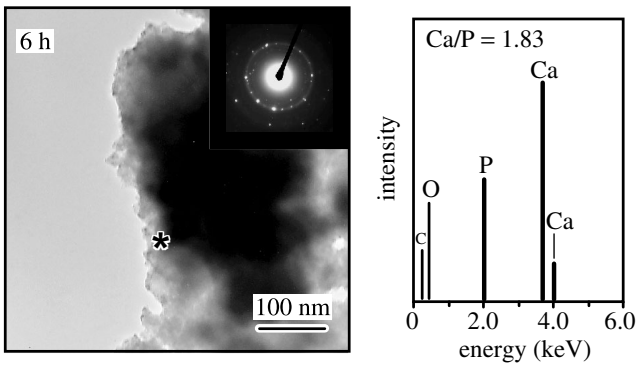

Figure 3. TEM–EDX profile of the surface of HA after soaking in SBF for 6 h (∗: centre of electron diffraction and EDX).

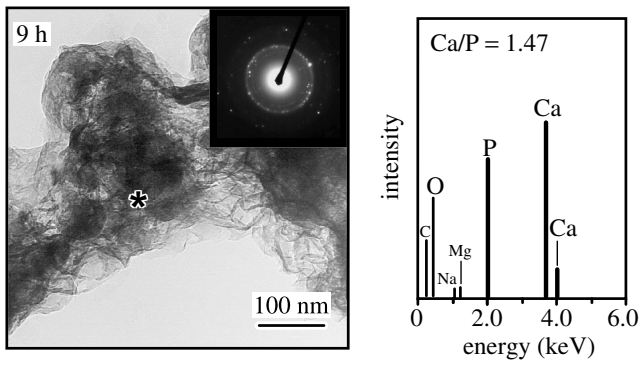

Figure 4. TEM–EDX profile of the surface of HA after soaking in SBF for 9 h (∗: centre of electron diffraction and EDX).

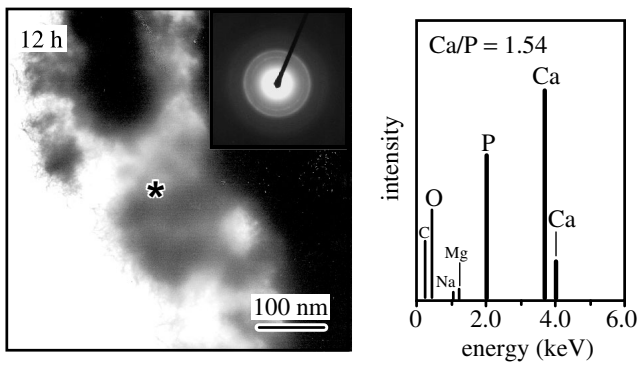

Figure 5. TEM–EDX profile of the surface of HA after soaking in SBF for 12 h (∗: centre of electron diffraction and EDX).

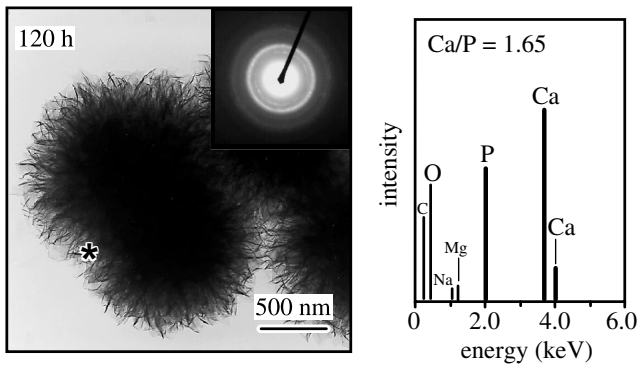

Figure 6. TEM–EDX profile of the surface of HA after soaking in SBF for 120 h (∗: centre of electron diffraction and EDX).

dim and broad ring patterns were revealed, decreasing the resolution of the dot patterns of the HA. After soaking for 6 h (see figure 3), this electron-lucent surface product became dense in the bulk and flat on the surface. While the Ca/P ratio increased further to 1.83, the electron diffraction patterns were apparently unchanged compared with those observed after 3 h. This indicates that a Ca-rich amorphous calcium phosphate (ACP) was formed on the HA up to 3 h and grew there with a further increase in the soaking time to 6 h.

After soaking for 9 h (see figure 4), the TEM observed a fibrous product on the HA. The EDX detected small amounts of Na and Mg in addition to Ca, P, O and C, and the Ca/P ratio decreased drastically to 1.47. The electron diffraction revealed broad ring patterns around the dim dot patterns of HA, which were not resolvable so as to be attributed to a crystalline phase. This fibrous product was therefore assumed to be a Ca-poor ACP, different from the Ca-rich ACP that was observed on the HA after 3–6 h.

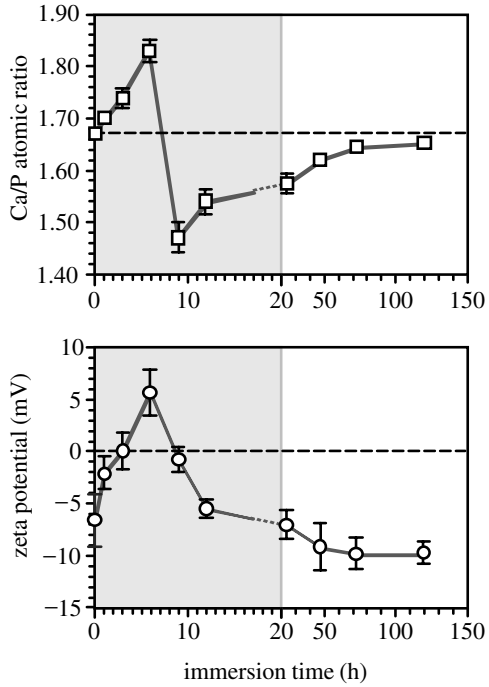

Figure 7. Ca/P atomic ratio and zeta potential of the surface of HA as a function of soaking time in SBF (note the scale of the soaking time).

After soaking for 12 h (see figure 5), the TEM observed a number of tiny needle-like precipitates on the top surface of the HA, where the EDX detected that the Ca/P ratio increased to 1.54. In the electron diffraction, resolvable ring patterns ascribed to the (002), (211) and (213) planes of crystalline apatite appeared instead of the dot patterns of the substrate HA, indicating that the apatite had finally formed on the HA surface. Thereafter with an increase in soaking time up to 120 h (see figure 6), these apatite crystals were observed to grow and assemble together in the form of needle-like particles. The Ca/P ratio increased to 1.65 and the ring diffraction patterns of the apatite became much more distinct. Specifically, these apatites were shown to incorporate Na and Mg, have a Ca/P ratio slightly lower than that of stoichiometric HA and reveal ring patterns in electron diffraction. These results indicate that the apatite produced on HA in SBF is a solid solution containing minor elements such as Na and Mg, and it is composed of low crystalline defective nanocrystallites. These characteristics are, in fact, those typically observed in biological apatite in bone tissue (Kokubo 1990, 1991; Hench 1991; Kim 2001; Ohtsuki *et al.* 1991; Ohura *et al.* 1991; Daculsi *et al.* 1990; Kitsugi *et al.* 1990).

Figure 7 shows the Ca/P atomic ratio and zeta potential of the surface of HA as a function of soaking time in SBF. The Ca/P ratio, which was initially 1.67, increased up to 1.83 in the soaking period 0–6 h, decreased to 1.47 in the next soaking period 6–9 h and then increased again to converge at 1.65 in the soaking period 9–120 h. The zeta potential showed a consonant change with the Ca/P ratio. The zeta potential of the HA was highly negative immediately after soaking, i.e. −6.47 mV. In the soaking period 0–6 h, the zeta potential increased to reveal a maximum positive value of +5.81 mV, then decreased to again reveal a negative value of −0.92 mV in the next soaking period 6–9 h and decreased to converge at around −10 mV in the soaking period 9–120 h.

4. DISCUSSION

The above TEM–EDX profiles and interpretations indicate that, after immersion in SBF, the HA undergoes three characteristic surface structural changes in the process of apatite formation on its surface. The first surface structural change is the formation of a Ca-rich ACP on the HA, which was shown to take place in the nominal soaking period 0–6 h. In view of the change in the Ca/P ratio, the formation of Ca-rich ACP is assumed to be a consequence of interaction of the HA surface specifically with the calcium ions in the SBF. The second surface structural change is the formation of Ca-poor ACP on the HA in the next soaking period 6–9 h. In this soaking period, the HA appears to use the Ca-rich ACP on its surface to interact with the phosphate ion in the fluid to form the Ca-poor ACP. The third surface structural change is the formation of apatite in the soaking period 9–12 h, in which the Ca-poor ACP on the HA appears to crystallize into apatite with bone mineral-like composition and structure. Thereafter with increased soaking time in SBF, the apatite was shown to grow, incorporating the calcium and phosphate ions in the SBF. The zeta potential indicates that the HA changes the surface potential, which was highly negative immediately after exposure to SBF, in a very consonant way during the above soaking periods of surface structural changes. The HA was shown to increase the surface potential to reveal a maximum positive charge when it was forming the Ca-rich ACP and to decrease it to again reveal a negative charge when it was forming the Ca-poor ACP. It then continued to decrease the surface potential whilst forming the apatite and then stabilized it at a constant negative charge.

The changes of bioactive surfaces during *in vitro* exposures have been documented in terms of the Ca/P ratio and surface potential in some of the literature. Hench (1991), Ogino & Hench (1980) and Ohtsuki *et al.* (1991, 1995) showed *in vitro* that the formation of apatite on Bioglass®-type glass and glass–ceramic A–W was preceded by the formation of ACP with a low Ca/P ratio. Lu *et al.* (2001) showed that on immersion in electrolyte solution with fibronectin, a Bioglass®-type glass reveals negative, positive and finally negative zeta potential with the increase in immersion time; the present authors also documented the same tendency of the zeta potential change using bioactive sodium titanate (Takadama *et al.* 2001b). The HA model in this study indicates, in fact, that bioactive surfaces would undergo the same sequence of changes in surface potential and Ca/P ratio, and suggests a correlation between the surface composition and potential.

Complementing the change in surface potential, the change in the surface structure of HA is due to the sequential process directed towards the formation of apatite, which reveals the electrostatic interaction of

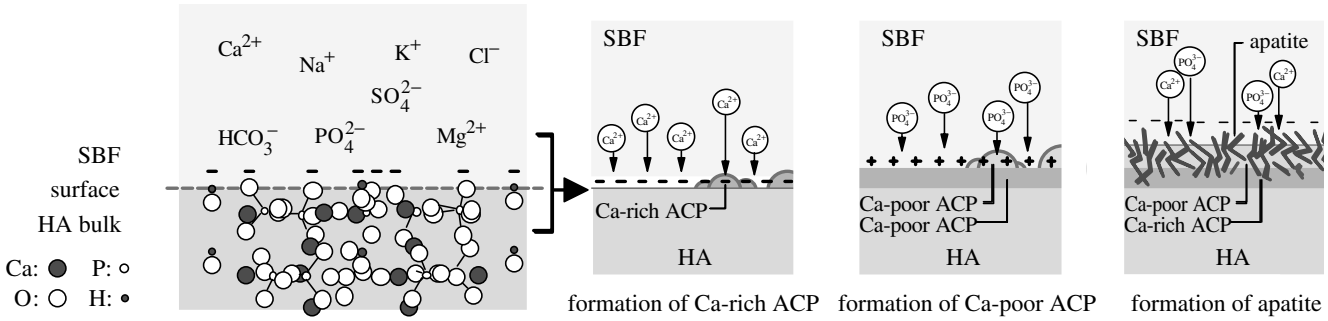

Figure 8. Schematic presentations of the origin of the negative charge on the HA surface (in case of the (100) projection of crystal structure), and the process of bone-like apatite formation thereon in SBF.

the HA surface with the calcium and the phosphate ions in the SBF. Figure 8 schematically summarizes the mechanism of bone-like apatite formation on HA in SBF, by indicating the processes of formation of the Ca-rich ACP incorporating calcium ions, the Ca-poor ACP incorporating phosphate ions and the apatite incorporating both the calcium and phosphate ions.

While the solubility of HA is extremely low in water, its iso-electric point, i.e. 5–7, is lower than the pH of the SBF, i.e. 7.4 (Bell *et al.* 1972; Somasundaran & Markovic 1998; Elliot 1994). On immersion in SBF, the HA could reveal a negative surface charge by exposing hydroxyl and phosphate units in its crystal structure (Bell *et al.* 1972; Somasundaran & Markovic 1998). The HA surface uses this negative charge to specifically gather the positive calcium ions in the fluid, thereby forming the Ca-rich ACP. This process is assumed to take place in consecutive accumulation of the calcium ions, which makes the Ca-rich ACP acquire and increase the positive charge. The Ca-rich ACP thereby relays the electrostatic interaction from the HA to use its positive charge for specifically gathering the negative phosphate ions in the fluid. The consequence is the formation of the Ca-poor ACP, which has been documented to take place in the process of apatite formation on various bioactive ceramics (Ebisawa *et al.* 1993; Ohtsuki *et al.* 1992; Kim *et al.* 1995, 1996b; Takadama *et al.* 2001a, 2001b; Coreño *et al.* 2001). The solubility of apatite is in fact lower than any other calcium phosphates in water, and therefore most of the calcium phosphates stabilize thermodynamically by transforming into a crystal phase of apatite in an aqueous environment. Namely, the Ca-poor ACP crystallizes into the apatite to form a stable surface phase in SBF. The SBF mimics the blood plasma in ion composition as well as in ion concentrations, which presents a metastable supersaturation with respect to the apatite (Ohtsuki *et al.* 1992; Neuman & Neuman 1958; Gamble 1967). Therefore, once formed on a bioactive surface in SBF, the apatite grows spontaneously consuming the calcium and phosphate ions, incorporating sodium, magnesium and carbonate ions, and thereby revealing bone mineral-like compositional and structural features.

5. CONCLUSION

On immersion and soaking in SBF, the synthetic HA was found to induce the formation of bone-like apatite on its surface through the formation of Ca-rich ACP in the early soaking period and the formation of Ca-poor ACP in the late soaking period. The formations of these two precursor ACPs are sequential consequences of electrostatic interactions of the HA surface with the calcium and the phosphate ions in the SBF. On exposure to SBF, the HA surface naturally reveals a negative charge, and thereby interacts with positive calcium ions in the fluid to form the Ca-rich ACP acquiring a positive charge. The Ca-rich ACP on the HA relays the following electrostatic interaction with negative phosphate ions in the fluid to form the Ca-poor ACP, which eventually crystallizes into bone-like apatite. This indicates that the biomineralization of bone-like apatite on the HA is a smart process involved with the electrostatic interaction of the HA surface with the calcium and the phosphate ions in blood plasma.

This work was supported in part by Korea Research Foundation Grant No. 2003-003-D00169.

REFERENCES

Bell, L. C., Posner, A. M. & Quirk, J. P. 1972 Surface charge characteristics of hydroxylapatite and fluorapatite. *Nature* **239**, 515–517.

Coreño, J., Martínez, A., Bolarín, A. & Sánchez, F. 2001 Apatite nucleation on silica surface: a zeta-potential approach. *J. Biomed. Mater. Res.* **57**, 119–125.

Daculsi, G., LeGeros, R. Z., Heughebaert, M. & Barbieux, I. 1990 Formation of carbonate-apatite crystals after implantation of calcium-phosphate ceramics. *Calcif. Tissue Int.* **46**, 20–27.

Ebisawa, Y., Kokubo, T., Ohura, K. & Yamamuro, T. 1993 Bioactivity of $CaO{\cdot}SiO_2$ glasses: *in vitro* evaluation. *J. Mater. Sci. Mater. Med.* **1**, 239–244.

Elliot, J. C. 1994 *Structure and chemistry of the apatites and other calcium orthophosphates*. Elsevier.

Filguerias, M. R., Torre, G. R. & Hench, L. L. 1993 Solution effects on the surface reaction of a bioactive glass. *J. Biomed. Mater. Res.* **27**, 445–453.

Gamble, J. 1967 *Chemical anatomy, physiological and pathology of extracellular fluid*. Harvard, MA: Harvard University Press.

Hench, L. L. 1991 Bioceramics: from concept to clinic. *J. Amer. Ceram. Soc.* **74**, 1487–1510.

Hench, L. L. 1998 Bioactive materials: the potential for tissue regeneration. *J. Biomed. Mater. Res.* **15**, 511–518.

Hench, L. L., Splinter, R. J., Allen, W. C. & Greenlee, T. K. 1971 Bonding mechanisms at the interface of ceramic prosthetic materials. *J. Biomed. Mater. Res. Symp.* **2**, 117–141.

Jarcho, M., Kay, J. L., Gumaer, R. H. & Drobeck, H. P. 1977 Tissue, cellular and subcellular events at bone–ceramic hydroxyapatite interface. *J. Bioeng.* **1**, 79–92.

Kim, H. M. 2001 Bioactive ceramics: challenges and perspectives. *J. Ceram. Soc. Jpn* **109**, S49–57.

Kim, H. M., Miyaji, F., Kokubo, T., Ohtsuki, C. & Nakamura, T. 1995 Bioactivity of Na_2O-CaO-SiO_2 glasses. *J. Am. Ceram. Soc.* **78**, 2405–2411.

Kim, H. M., Miyaji, F., Kokubo, T. & Nakamura, T. 1996a Preparation of bioactive Ti and its alloys via simple chemical surface treatment. *J. Biomed. Mater. Res.* **32**, 409–417.

Kim, H. M., Miyaji, F., Kokubo, T., Kobayashi, M. & Nakamura, T. 1996b Bioactivity of M_2O-TiO_2-SiO_2 (M = Na, K) glasses: an *in vitro* evaluation. *Bull. Chem. Soc. Japan* **69**, 2387–2394.

Kitsugi, T., Yamamuro, T. & Kokubo, T. 1990 Analysis of A–W glass–ceramic surface by micro-beam X-ray diffraction. *J. Biomed. Mater. Res.* **24**, 259–273.

Kokubo, T. 1990 Surface chemistry of bioactive glass–ceramics. *J. Non-Cryst. Solids* **120**, 138–151.

Kokubo, T. 1991 Recent progress in glass-based materials for biomedical applications. *J. Ceram. Soc. Jpn (Seramikkusu Ronbunshi)* **99**, 965–973.

Kokubo, T. 1992 Bioactivity of glasses and glass–ceramics. *Bone-bonding biomaterials* (ed. P. Ducheyne, T. Kokubo & C. A. Blitterswijk), pp. 31–46. Leidendorp: Reed Healthcare Communications.

Kokubo, T., Shigematsu, M., Nagashima, Y., Tashiro, M., Nakamura, T., Yamamuro, T. & Higashi, S. 1982 Apatite- and wollastonite-containing glass–ceramics for prosthetic application. *Bull. Inst. Chem. Res. Kyoto Univ.* **60**, 260–268.

Kokubo, T., Kushtani, H., Ebisawa, Y., Kitsugi, T., Kotani, S., Ohura, K. & Yamamuro, T. 1989 Apatite formation on bioactive ceramics in body environment. *Bioceramics* (ed. H. Oonishi, H. Aoki & K. Sawai), vol. 1, pp. 157–162. Tokyo: Ishiyaku Euro America.

Kokubo, T., Kushitani, H., Sakka, S., Kitsugi, T. & Yamamuro, T. 1990 Solution able to reproduce *in vivo* surface-structure changes in bioactive glass–ceramic A–W. *J. Biomed. Mater. Res.* **24**, 721–734.

Kokubo, T., Kim, H. M. & Kawashita, M. 2003 Novel bioactive materials with different mechanical properties. *Biomaterials* **24**, 2161–2175.

Li, P., Ohtsuki, C., Kokubo, T., Nakanishi, K., Soga, N., Nakamura, T. & Yamamuro, T. 1992 Apatite formation induced on silica gel in a simulated body fluid. *J. Am. Ceram. Soc.* **75**, 2094–2097.

Li, P., Ohtsuki, C., Kokubo, T., Nakanishi, K., Soga, N., Nakamura, T., Yamamuro, T. & de Groot, K. 1994 A role of hydrated silica, titania and alumina in forming biologically active bone-like apatite on implant. *J. Biomed. Mater. Res.* **28**, 7–15.

Lu, H. H., Pollack, S. R. & Ducheyne, P. 2001 45S5 bioactive glass surface charge variations and the formation of surface calcium phosphate layer in a solution containing fibronectin. *J. Biomed. Mater. Res.* **54**, 454–461.

Neo, M., Kotani, S., Nakamura, T., Yamamuro, T., Ohtsuki, C., Kokubo, T. & Bando, Y. 1992 A comparative study of ultrastructure of the interface between four kinds of surface-active ceramic and bone. *J. Biomed. Mater. Res.* **26**, 1419–1432.

Neo, M., Nakamura, T., Ohtsuki, C., Kokubo, T. & Yamamuro, T. 1993 Apatite formation on three kinds of bioactive materials at an early stage *in vivo*: a comparative study by transmission electron microscopy. *J. Biomed. Mater. Res.* **27**, 999–1006.

Neuman, W. & Neuman, M. 1958 *The chemical dynamics of bone mineral*. Chicago, IL: University of Chicago Press.

Ogino, M. & Hench, L. L. 1980 Formation of calcium phosphate films on silicate glasses. *J. Biomed. Mater. Res.* **38** & **39**, 673–678.

Ohtsuki, C., Kushitani, H., Kokubo, T., Kotani, S. & Yamamuro, T. 1991 Apatite formation on the surface of Ceravital-type glass–ceramic in the body. *J. Biomed. Mater. Res.* **25**, 1363–1370.

Ohtsuki, C., Kokubo, T. & Yamamuro, T. 1992 Mechanism of apatite formation on CaO-SiO_2-P_2O_5 glasses in a simulated body fluid. *J. Non-Cryst. Solids* **143**, 84–92.

Ohtsuki, C., Aoki, Y., Kokubo, T., Bando, Y., Neo, M. & Nakamura, T. 1995 Transmission electron microscope observation of glass–ceramic A–W and apatite layer formed on its surface in a simulated body fluid. *J. Ceram. Soc. Jpn* **103**, 449–454.

Ohura, K., Yamamuro, T., Nakamura, T., Kokubo, T., Ebisawa, Y., Kotoura, Y. & Oka, M. 1991 Bone-bonding ability of P_2O_5-free CaO·SiO_2 glasses. *J. Biomed. Mater. Res.* **25**, 357–365.

Somasundaran, P. & Markovic, B. 1998 Interfacial properties of calcium phosphate. *Calcium phosphate in biological and industrial system* (ed. Z. Amjad), pp. 85–101. Uetikon-Zuerich, Switzerland: Trans Tech Publications.

Takadama, H., Kim, H. M., Kokubo, T. & Nakamura, T. 2001a Mechanism of biomineralization of apatite on a sodium silicate glass: TEM–EDX study *in vitro*. *Chem. Mater.* **13**, 1108–1113.

Takadama, H., Kim, H. M., Kokubo, T. & Nakamura, T. 2001b TEM–EDX study of the mechanism of bonelike apatite formation on bioactive titanium metal in simulated body fluid. *J. Biomed. Mater. Res.* **57**, 441–448.

Takadama, H., Kim, H. M., Kokubo, T. & Nakamura, T. 2002 X-ray photoelectron spectroscopy study on the process of apatite formation on a sodium silicate glass in simulated body fluid. *J. Am. Ceram. Soc.* **85**, 1933–1936.

van de Ven, T. G. M. 1989 *Colloidal hydrodynamics*, p. 1. Academic.